Published online January 2, 2004

Nucleic Acids Research, 2004, Vol. 32, No. 1 ***169–178***
DOI: 10.1093/nar/gkg925

Domain mapping of the Rad51 paralog protein complexes

Kristi A. Miller, Dorota Sawicka, Daniel Barsky and Joanna S. Albala*

Biology and Biotechnology Research Program, Lawrence Livermore National Laboratory, 7000 East Avenue, L-448, Livermore, CA 94550, USA

Received August 15, 2003; Revised and Accepted October 21, 2003

ABSTRACT

The five human Rad51 paralogs are suggested to play an important role in the maintenance of genome stability through their function in DNA double-strand break repair. These proteins have been found to form two distinct complexes *in vivo*, Rad51B–Rad51C–Rad51D–Xrcc2 (BCDX2) and Rad51C–Xrcc3 (CX3). Based on the recent *Pyrococcus furiosus* Rad51 structure, we have used homology modeling to design deletion mutants of the Rad51 paralogs. The models of the human Rad51B, Rad51C, Xrcc3 and murine Rad51D (mRad51D) proteins reveal distinct N-terminal and C-terminal domains connected by a linker region. Using yeast two-hybrid and co-immunoprecipitation techniques, we have demonstrated that a fragment of Rad51B containing amino acid residues 1–75 interacts with the C-terminus and linker of Rad51C, residues 79–376, and this region of Rad51C also interacts with mRad51D and Xrcc3. We have also determined that the N-terminal domain of mRad51D, residues 4–77, binds to Xrcc2 while the C-terminal domain of mRad51D, residues 77–328, binds Rad51C. By this, we have identified the binding domains of the BCDX2 and CX3 complexes to further characterize the interaction of these proteins and propose a scheme for the three-dimensional architecture of the BCDX2 and CX3 paralog complexes.

INTRODUCTION

Human Rad51, like its bacterial homolog, RecA, catalyzes the repair of DNA double-strand breaks through the process of homologous recombination (1–4). In higher eukaryotes, five proteins that share ~25% amino acid sequence identity with Rad51 have been identified. These Rad51 paralogs, Rad51B (Rad51L1), Rad51C (Rad51L2), Rad51D (Rad51L3), Xrcc2 and Xrcc3 (5–13), have presumably arisen through gene duplication and may have acquired new cellular functions distinct from Rad51. Embryonic lethality of knockout mice for Rad51B, Rad51D and Xrcc2 demonstrates that these proteins play an essential function in development (14–16). It has also been demonstrated that these proteins are critical for genome stability as evidenced by the sensitivity of individual DT40 chicken B-cell knockout mutants and CHO mutants cell lines to ionizing radiation and DNA-damaging agents (7,10,17–19).

Yeast two-hybrid experiments (20) and co-immunoprecipitation have revealed heterologous interactions between the paralogs, and the following pair-wise complexes have been observed: Rad51B–Rad51C (21,22), Rad51C–Rad51D (20), Rad51D–Xrcc2 (23,24), Rad51C–Xrcc3 (CX3) (25,26). A larger quaternary complex, Rad51B–Rad51C–Rad51D–XRCC2 (BCDX2), has also been identified *in vitro* and *in vivo* (22,25–27). In addition, these paralog complexes bind DNA and demonstrate weak ATPase activity (21,24,25,28,29). Evidence suggests that these paralog complexes may mediate the strand exchange activity of Rad51 during the process of homologous recombination (21,28). Furthermore, Rad51B has been shown to bind to Holliday junctions as well as to interact with histones *in vitro* (30,31). Identification of the protein–protein interactions underlying heterologous complex formation will further elucidate the biological function of the paralog proteins.

In order to determine the interacting regions between each paralog in the BCDX2 and CX3 complexes, deletion mutations can be designed based on knowledge of the monomeric structure of each paralog. As no three-dimensional structure has been solved for any individual paralog protein or complex, crystal structures of related proteins can be used as structural templates to build three-dimensional models of these proteins. An X-ray crystal structure of RecA from *Escherichia coli* (32,33), an NMR structure of the N-terminus of human Rad51(34), and an X-ray crystal structure of a C-terminal fragment of human Rad51 bound to a fragment of BRCA2 (35) are available in the Protein Data Bank (PDB) for use as structural templates. Previously, the RecA structure alone was used to create homology models of *Saccharomyces cerevisiae* Rad51 (36) and human Xrcc3 (37), but these models are limited by low sequence identity of ~15% between RecA and Rad51 as well as a much shorter N-terminus in RecA as compared with Rad51 and some of its paralogs. Since the experimental structures described above are incomplete relative to the paralogs, the recent determination of the full-length *Pyrococcus furiosus* Rad51 (*Pf*Rad51) provides a more

*To whom correspondence should be addressed. Tel: +1 925 422 6442; Fax: +1 925 424 6605; Email: albala1@llnl.gov

The authors wish it to be known that, in their opinion, the first two authors should be regarded as joint First Authors

accurate structure for modeling the Rad51 paralogs (38). The *Pf*Rad51 protein contains ~45% sequence identity with human Rad51 and between 18 and 28% sequence identity with the paralogs. The *Pf*Rad51 crystal structure reveals a clear N-terminal domain separated by a 'linker' region of approximately 17 residues from a large C-terminal domain.

We have used an advanced sequence analysis procedure, PSI-BLAST-ISS (39), and comparative modeling (40,41) to generate three-dimensional structures of the Rad51 paralogs based on the *Pf*Rad51 crystal structure. We have used these structures to delineate the N-terminal, C-terminal and linker domains of the Rad51 paralogs for the generation of deletion mutants to use for domain mapping and analysis of complex binding.

MATERIALS AND METHODS

Plasmid construction

Yeast two-hybrid plasmid constructs for full-length human Rad51B, Rad51C and Xrcc3 were the kind gift of Dr David Schild (Lawrence Berkeley National Laboratory; Berkeley, CA). The full-length murine Rad51D cDNA construct was the kind gift of Dr Doug Pittman (Medical College of Ohio, Toledo, OH). The murine Rad51D sequence was used in these studies as it had optimal activity with Rad51C and Xrcc2 by yeast two-hybrid analysis. The mRad51D construct contains an N-terminal hemaglutinin tag and was cloned into the pGADT7 yeast two-hybrid vector using restriction sites EcoRI and BamHI. I.M.A.G.E. clone 5801996 containing the full-length cDNA for Xrcc2 was obtained from the I.M.A.G.E cDNA collection (42), amplified by PCR with primers containing EcoRI and BamHI sequences, and subsequently cloned into the pGADT7 and pGBKT7 yeast two-hybrid vectors. Deletion constructs were made using the QuikChange mutagenesis kit (Qiagen, Valencia, CA) and verified by sequencing (Biotech Core, Mountain View, CA).

Yeast two-hybrid analysis

The Matchmaker yeast two-hybrid kit was used as per the manufacturer's instructions (Clontech, Palo Alto, CA). Briefly, the yeast strain AH109 was co-transformed with various combinations of the paralog proteins cloned into the DNA binding domain and activating domain vectors and plated on minimal media lacking leucine and tryptophan but containing 5-bromo-4-chloro-3-indolyl α-D-galactopyranoside (X-α-Gal; Sigma-Aldrich, St Louis, MO) which allowed for detection of protein–protein interactions directly on the plate. In addition, transformed yeast were also plated on minimal media lacking leucine, tryptophan and histidine to select for positive protein–protein interactions. To quantitate the interactions between any two protein combinations, liquid β-galactosidase assays were performed on co-transformed yeast colonies using *O*-nitrophenol-β-D-galactopyranoside (ONPG; Sigma-Aldrich) as a substrate as outlined in the yeast protocols handbook (Clontech). Briefly, 5 ml of yeast were grown overnight in minimal medium lacking leucine and tryptophan. Then, 2 ml of yeast were transferred to 50 ml conical tubes containing 8 ml of yeast extract, peptone and dextrose, supplemented with adenine (YPDA) medium and grown with shaking for 3 h. The optical density (OD) at 600 nm was determined for each sample. Three aliquots of 1.5 ml of each sample were dispensed into microcentrifuge tubes, i.e. the triplicates for each experiment. Cells were centrifuged for 2 min at 10 000 *g* and washed with 1 ml of Z buffer (16.1 g/l $NaHPO_4{\cdot}7H_2O$, 5.5 g/l $NaHPO_4{\cdot}H_2O$, 0.75 g/l KCl, 0.246 g/l $MgSO_4{\cdot}7H_2O$). Cells were then resuspended in 100 µl of Z buffer and were subjected to three cycles of freeze–thaw. To each tube, 700 µl of Z buffer plus Tris[2-carboxyethyl] phosphine, used as a reducing agent, and 160 µl of 4 mg/ml ONPG was added and the tubes were incubated at 30°C until a yellow color developed. The reaction was stopped by adding 400 µl of 1 M $NaCO_3$ and the samples were centrifuged at 14 000 *g* for 10 min. The OD of the samples was obtained at 420 nm and β-galactosidase units were calculated. All yeast two-hybrid assays were performed with constructs in both the GAL4 DNA binding and transcription activating domains to reduce the possibility of spurious data.

Baculovirus generation and infection

Baculovirus transfer vectors containing full-length and deletion constructs of Rad51B and Rad51C were created by PCR from the yeast two-hybrid vectors with primers to create AscI and FseI restriction enzyme sites on the inserts. Inserts were cloned into a modified pBacPAK9 vector (Clontech) containing an N-terminal His tag. Vectors were co-transfected with linearized baculoviral DNA (Baculogold; Pharmingen, San Diego, CA) into *Sf*21 cells and recombinant virus was generated, amplified three times, and tested for recombinant protein expression by SDS–PAGE and western blot analysis. The cDNA containing Xrcc3 (a kind gift from Larry Thompson, LLNL) was amplified by PCR and cloned into the pFastBacHT vector (Invitrogen, Carlsbad, CA) using BamHI and HindIII restriction enzyme sites. Baculovirus for His-tagged Xrcc3 was generated using the Bac-to-Bac™ system as per the manufacturer's instructions (Invitrogen).

*Sf*21 cells were maintained in SFMII media (Invitrogen) at 28°C. To produce recombinant protein, 1.25×10^6 cells/ml were seeded into 96 deep-well plates at a total volume of 1.5 ml and aerated with magnetic balls using a Carousel Magnetic Levitation stirrer (V&P Scientific, San Diego, CA). Cells were co-infected with virus encoding the His-tagged full-length protein or fragments of Rad51B or Rad51C along with the corresponding Glu-tagged partner (22). The His-tagged Xrcc3 virus was also co-infected with a His-tagged Rad51C virus. Cells were harvested after 36–44 h by centrifugation at 1000 *g* for 5 min. After centrifugation, the supernatant was removed, the cells were resuspended in hypotonic lysis buffer (20 mM Tris pH 7.5, 1 mM $MgCl_2$, 0.5% NP-40 and protease inhibitors), incubated on ice for 10 min, vortexed for 30 s, and the extract was clarified by centrifugation at 14 000 *g* for 3 min. Extracts were then brought to 0.1 M NaCl prior to immunoprecipitation.

Immunoprecipitation and western blot analysis

Approximately 400 µg of His-tagged Rad51B or Rad51C protein was immunoprecipitated by incubation with anti-His antibody covalently linked to agarose beads (Sigma-Aldrich) for 1 h with rocking at 4°C. In the Rad51C–Xrcc3 experiments, both proteins were His tagged and therefore immunoprecipitation was performed using an Xrcc3-specific antibody

(Santa Cruz Biotechnology, Santa Cruz, CA). Antibody-linked agarose beads and lysates were gently centrifuged at 1000 *g* for 2 min. Supernatant was removed and the beads were washed three times with 500 µl of cold lysis buffer. Immunoprecipitations performed with anti-His antibody-linked agarose beads were first eluted in 0.1 M imidazole. Samples were then resuspended in SDS–PAGE loading dye, boiled for 5 min, centrifuged and the supernatant electrophoresed by SDS–PAGE using precast 4–20% gels (Gradipore Inc., Hawthorne, NY). Gels were transferred to polyvinylidene difluoride (PVDF; Bio-Rad Laboratories, Hercules, CA) and blotted in 5% PBS milk with the appropriate antibody for 1 h. Anti-His monoclonal antibody (Sigma-Aldrich) was diluted 1:3000, while anti-His goat polyclonal antibody (Novus Biologicals, Littleton, CO) was used at 1:1000 dilution. Rad51B rabbit polyclonal antibody and Rad51C monoclonal antibody were used at 1:1000 (22). Blots were then washed three times in 0.1% TBS-Tween for 10 min. Secondary antibody bovine anti-goat, goat anti-mouse and goat anti-rabbit HRP were all diluted 1:3000 in PBS milk and then blots were washed three times in 0.1% TBS-Tween and detected by enhanced chemiluminescence (Amersham Biosciences, Piscataway, NJ).

Computational modeling of the Rad51 paralogs

For homology modeling, sequence alignments were obtained using the PSI-BLAST-ISS procedure developed by C. Venclovas (39). Briefly, two iterations of PSI-BLAST were performed using the non-redundant database (43) on each Rad51 paralog: human Rad51B, Rad51C, Xrcc2, Xrcc3 and mRad51D. Sequences that appeared with an expectation value less than 10^{-40} were selected and then further limited to sequences that had <60% sequence identity to each other. The resulting list of sequences was then used to generate subsequent PSI-BLAST searches, each consisting of five rounds. The fifth round of PSI-BLAST was used to extract the resulting alignment of the target (Rad51 paralogs) and template (*Pf*Rad51) sequence using the SEALS package (44) combined with in-house Perl scripts (C. Venclovas). The variability in the alignment between the target and template was analyzed and the dominant alignment variant was used to generate three-dimensional models using Modeler 6.1 (45). In regions, however, where the alignment was ambiguous (no variation was dominant), secondary structure prediction using PSI-PRED was used to choose an alignment (46). Secondary structure was also used to shift the alignment in places where the PSI-BLAST alignment would otherwise have produced a break in a predicted α-helix or β-strand. The crystal structure of the archaeal Rad51 protein from *P.furiosus* was used as the main template for model building, PDB accession code 1pzn (47). An insertion in Rad51C relative to *Pf*Rad51, residues 164–212 [indicated by the lower red arrow in the Rad51C model shown in Fig. S1 (available as Supplementary Material at NAR Online)], was modeled using the helicase domain of the gene 4 protein of bacteriophage T7, PDB accession code 1cr0 (48), residues 76–124. An insertion in Rad51B, residues 253–311 (indicated by the green arrow in the Rad51B model shown in Fig. S1), was modeled based on PDB entry 1db3, residues 125–181. This PDB structure was chosen from a list of proteins structurally related to RecA which had a similar length insertion as compared with human Rad51, identified through the Fold Classification based on Structure-Structure alignment of Proteins (FSSP) server (49). Other insertion regions were generated automatically by the Modeler program (45). The Sidechain Replacement with a Rotamer Library (SCWRL) program was used to build side chains in each model (50). To assess the quality of the final models, ProsaII *Z*-scores (43) were calculated (see Results).

RESULTS

In order to design deletion mutants for domain mapping of the BCDX2 and CX3 protein complexes, we derived homology models for the Rad51 paralogs from our sequence alignments and the *P.furiosus* Rad51 crystal structure. The *Pf*Rad51 protein contains ~45% sequence identity to human Rad51 and between 18 and 28% sequence identity to the Rad51 paralogs; thus, a closer sequence identity is found between the paralogs and *Pf*Rad51 as compared with RecA, which has been previously used in modeling *Sc*Rad51 (36) and Xrcc3 (37), making *Pf*Rad51 the most accurate structure that can thus far be used to model the Rad51 paralogs. The *Pf*Rad51 crystal structure reveals distinct N-terminal and C-terminal domains, separated by a 'linker' region. Secondary structure prediction, sequence alignment and model building suggest that four of the paralogs, with the exception of Xrcc2, possess an N-terminal domain of some 60–80 residues, similar to *Pf*Rad51. By way of contrast, RecA contains a single α-helix (approximately 20 residues) at its N-terminus compared with the four-helix bundle at the N-terminus of *Pf*Rad51. Thus, the *Pf*Rad51 structure provides a more complete template on which to model the Rad51 paralogs.

The sequence alignments of all the paralogs relative to *Pf*Rad51 and human Rad51 are given in Figure 1. These alignments were used to create models of the paralogs, all of which are shown in Figure S1 (available as Supplementary Material at NAR Online). Representative of all the models, the model for Rad51B is shown in Figure 2, and reveals the N- and C-terminal domains separated by a linker region, which ends just past residue 75 in Rad51B (circled in Fig. 2). The models for the other paralogs are similar with subtle differences due to the insertion regions that are unique to a particular paralog and in Figure S1 are color coded by certainty of the alignment, red representing no variation in the alignment, green representing some variation, and blue representing an insertion region relative to the *Pf*Rad51 template (Fig. S1). ProsaII *Z*-scores for each model have been compared with the template *Pf*Rad51 structure in order to assess the overall quality of the models (51). A ProsaII *Z*-score of a model that is within two to three units of its corresponding template's *Z*-score indicates a sound sequence alignment. The ProsaII score for the full-length *Pf*Rad51 crystal structure is –10.5. The ProsaII scores for each model are as follows: Rad51B, –9.6; Rad51C, –8.2; mRad51D, –8.4; and Xrcc3, –8.2. Since Xrcc2 lacks an N-terminal α-helical bundle, its ProsaII score, –6.6, is compared with that of $PfRad51_{90–349}$, which is –9.2. Secondary structure assignment by the DSSP method (52) for *Pf*Rad51 is shown above the sequence alignment in Figure 1 and features four α-helices in the N-terminus and eight α-helices and 11 β-strands in the C-terminal region. The N-terminal region of human Rad51 has been shown to bind

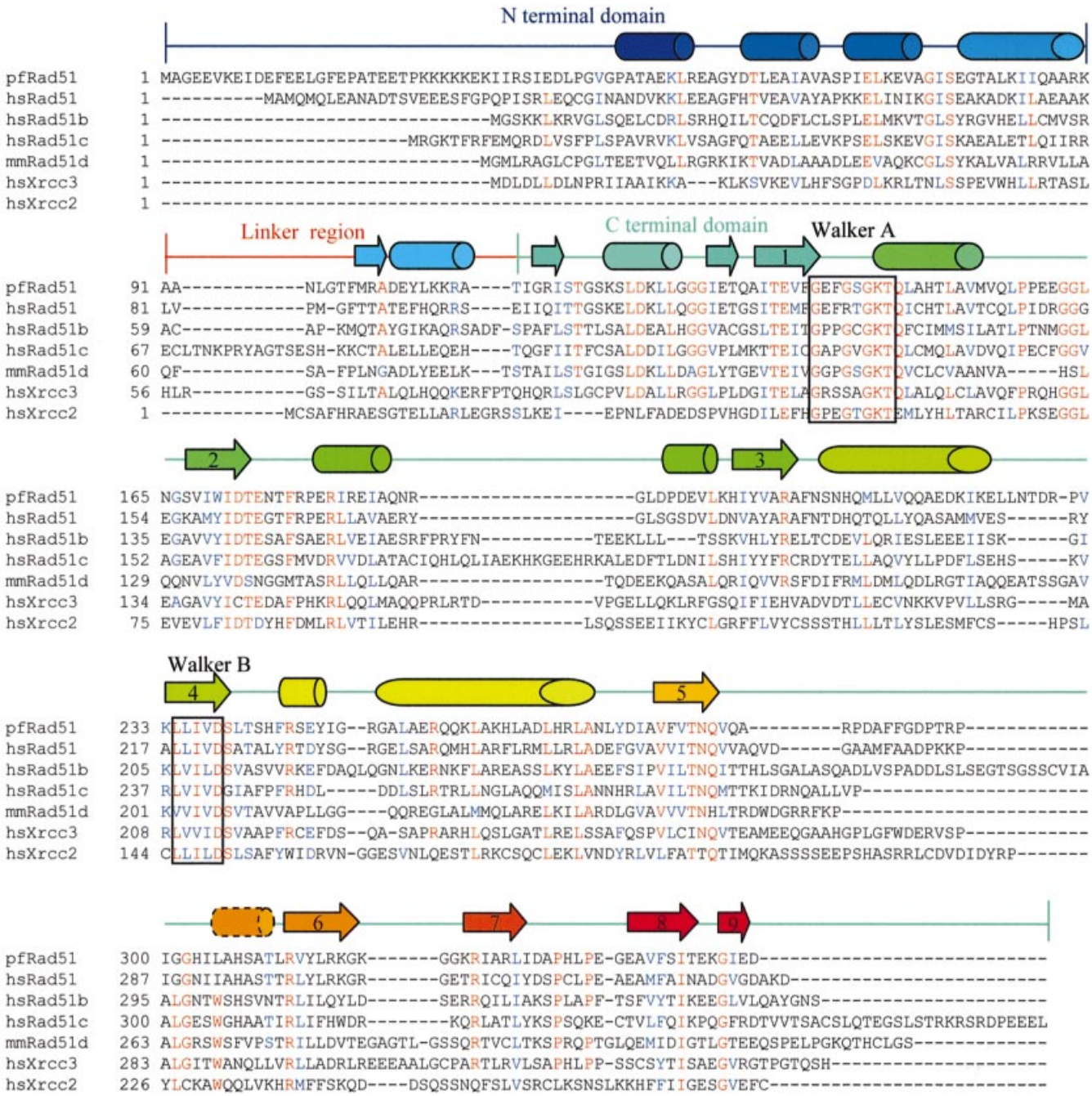

Figure 1. Sequence alignment of *P.furiosus* (Pf) and human (Hs) Rad51, Rad51B, Rad51C, *murine* (Mm) Rad51D, and human Xrcc2 and Xrcc3. Secondary structure for *Pf*Rad51 is shown schematically above the amino acid sequences, with cylinders for α-helices and arrows for β-strands, colored from blue to red, from the N- to the C-terminus, respectively. The helix preceding strand six, shown with a dashed line, is predicted in the Rad51 paralogs using PSI-PRED (46), but is absent in the *Pf*Rad51 crystal structure. Thin, horizontal colored lines indicate approximate regions of the N-terminal domain, the linker region, and the C-terminal domain by the colors blue, red and turquoise, respectively. The Walker A and Walker B ATP binding motifs are indicated by rectangles.

DNA (34), whereas the C-terminal region contains the canonical Walker A and B boxes for hydrolysis of ATP (53).

In order to identify which region of the Rad51B protein interacts with Rad51C, several deletion mutants of Rad51B were tested for binding against the full-length Rad51C protein by yeast two-hybrid analysis. As shown in Figure 3A, the N-terminal fragments $Rad51B_{1–75}$ and $Rad51B_{1–115}$ bind to Rad51C while the complementary fragments $Rad51B_{76–350}$ and $Rad51B_{116–350}$ did not bind to Rad51C, nor did $Rad51B_{1–243}$ and $Rad51B_{243–350}$. From the homology modeling, it seems likely that the larger N-terminal fragment $Rad51B_{1–243}$ cannot produce a properly folded protein, invalidating the binding assay. The sequence alignment shows that $Rad51B_{1–243}$ is truncated within the helix preceding strand 5, while

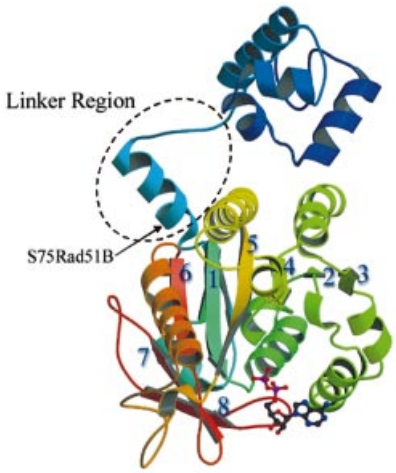

Figure 2. A ribbon diagram of a model of Rad51B is shown. This structure is representative of the topology for the Rad51C, mRad51D and Xrcc3 proteins. The blue to red color coding is from the N- to C-terminus of Rad51B as in the secondary structure assignment shown in Figure 1 for *P.furiosus* Rad51. β-Strands are labeled from 1–8 (see Fig. 1). ADP, shown in blue, black and pink ball and stick representation, is modeled from the RecA crystal structure, PDB accession code 1rea (32). This depiction was created using Molscript (55) and Raster3D (56). The linker region and restriction enzyme digest site, S75, is circled in a dashed outline. The coil and helix, colored in orange, between strands 5 and 6, were modeled based on amino acid residues 125–181 of PDB structure 1db3 (57), which was identified using FSSP (49).

$Rad51B_{243–350}$ includes the eight residues preceding strand 5 to the end of the protein. A structure-based analysis using the model of Rad51B suggests that these fragments may result in misfolded proteins since a portion of the internal β-sheet is missing in both fragments. Inspection of the Rad51B model (Fig. 2) clearly shows that the β-strands do not fold in a sequential numerical order 1–2–3–4–5–6–7–8; instead the order is 8–7–6–1–5–4–2–3 as in *Pf*Rad51. Therefore, if fragments $Rad51B_{1–243}$ missing strands 5–8 and $Rad51B_{243–350}$ missing strands 1–4 cannot produce a properly folded protein, then the yeast two-hybrid assay will not yield positive results. Furthermore, the smaller fragment $Rad51B_{1–60}$ also did not bind to Rad51C, suggesting that residues 60–75, the putative Rad51B linker region, are critical for the interaction of Rad51B with Rad51C. Surprisingly, even though the linker is present in $Rad51B_{57–350}$, this fragment did not bind to Rad51C, suggesting that residues 60–75 may be functional only when attached to the N-terminal domain rather than the C-terminal domain of Rad51B.

Similarly, several deletion mutants of Rad51C were tested against the full-length Rad51B protein (Fig. 3B). Of these, only the $Rad51C_{79–376}$ was found to bind the full-length Rad51B protein and the reciprocal fragment $Rad51C_{1–79}$ did not bind. Again, we hypothesize that removal of an internal β-strand of the Rad51C protein prevents the core β-sheet of the protein from properly folding, resulting in an apparent lack of binding activity. Indeed, fragments that do not contain a complete β-sheet $Rad51C_{1–246}$, $Rad51C_{1–145}$, $Rad51C_{145–376}$ and $Rad51C_{264–376}$ showed no binding activity (Fig. 3B). In addition, fragments $Rad51C_{1–96}$, $Rad51C_{96–376}$, $Rad51C_{1–285}$ and $Rad51C_{285–376}$ did not show activity against Rad51B by the yeast two-hybrid assay (data not shown). The deletion mutants $Rad51C_{1–285}$ and $Rad51C_{285–376}$ were designed to dissect the β-sheet within the C-terminus of Rad51C to examine how much of this β-sheet must remain intact for the binding of Rad51C to Rad51B. $Rad51C_{1–285}$ includes strands 1–5, while $Rad51C_{285–376}$ includes strands 6–9 of Rad51C. Such a dissection would disrupt the hydrogen bonding between only one pair of β-strands. In contrast, the non-binding deletions at amino acid residues 145 and 246 of Rad51C would break the hydrogen bonds between two pairs of β-strands, potentially resulting in even greater instability within the protein core. Moreover, since no binding was observed for either $Rad51C_{1–285}$ or $Rad51C_{285–376}$ in the yeast two-hybrid assay, we infer that a complete β-sheet is important in maintaining the overall fold of the protein.

Additional deletion mutants $Rad51C_{1–96}$ and $Rad51C_{96–376}$ were designed to determine whether the linker region was essential for binding to Rad51B and so these fragments separate the putative linker from the C-terminal domain. Although neither the $Rad51C_{1–96}$ nor the $Rad51C_{96–376}$ fragment bound full-length Rad51B, we infer from the $Rad51C_{79–376}$ fragment that binds Rad51B, that the linker region of Rad51C, residues 79–96, must be present on the C-terminus of Rad51C for proper interaction with the Rad51B protein. Henceforth, use of the phrase 'C-terminal domain' with respect to Rad51C will include this linker region (i.e. residues 79–376).

The N- and C-terminal domain fragments of the Rad51B and Rad51C proteins that tested positive for binding to their respective full-length protein partner were tested for binding to one another in the yeast two-hybrid assay (Fig. 3C). Only the N-terminal fragment $Rad51B_{1–75}$ bound to the C-terminal fragment $Rad51C_{79–376}$ with similar strength as compared with the binding of the $Rad51B_{1–75}$ to the full-length Rad51C protein. Similarly, the $Rad51C_{79–376}$ fragment bound to the $Rad51B_{1–75}$ fragment with the same strength as with full-length Rad51B (Fig. 3C). This result provides a clear demonstration of the N-terminal domain of Rad51B binding to the C-terminal domain of Rad51C.

To confirm these findings, the N- and C-terminal fragments of Rad51B and Rad51C were cloned into baculoviral constructs, expressed in insect cells, and tested for protein–protein interactions by co-immunoprecipitation. A Glu-tagged Rad51C construct was co-infected with either full-length Rad51B or the Rad51B fragments, each of which contained an N-terminal His tag. Figure 4A(I) shows that all of the Rad51B fragments were expressed in the co-infections. Figure 4A(II) shows equal Rad51C expression in each co-infection with the Rad51B fragments. Immunoprecipitation using an anti-His antibody showed that only the full-length Rad51B or $Rad51B_{1–75}$ (and not $Rad51B_{76–350}$) binds to Rad51C (Fig. 4A, III). Insect cells infected with Rad51C alone did not immunoprecipitate the Glu-tagged Rad51C with the anti-His antibody which demonstrates the specificity of the anti-His antibody only for His-tagged proteins. In the reverse experiment, full-length, His-tagged Rad51C or His-tagged Rad51C N- and C-terminal fragments were co-expressed with Glu-tagged full-length Rad51B (Fig. 4B, I and II). Using an anti-His antibody for immunoprecipitation of the Rad51C proteins, Rad51B co-precipitated only with full-length Rad51C or $Rad51C_{79–376}$ (Fig. 4B, III). The Glu–Rad51B expressed alone was not immunoprecipitated with the anti-His

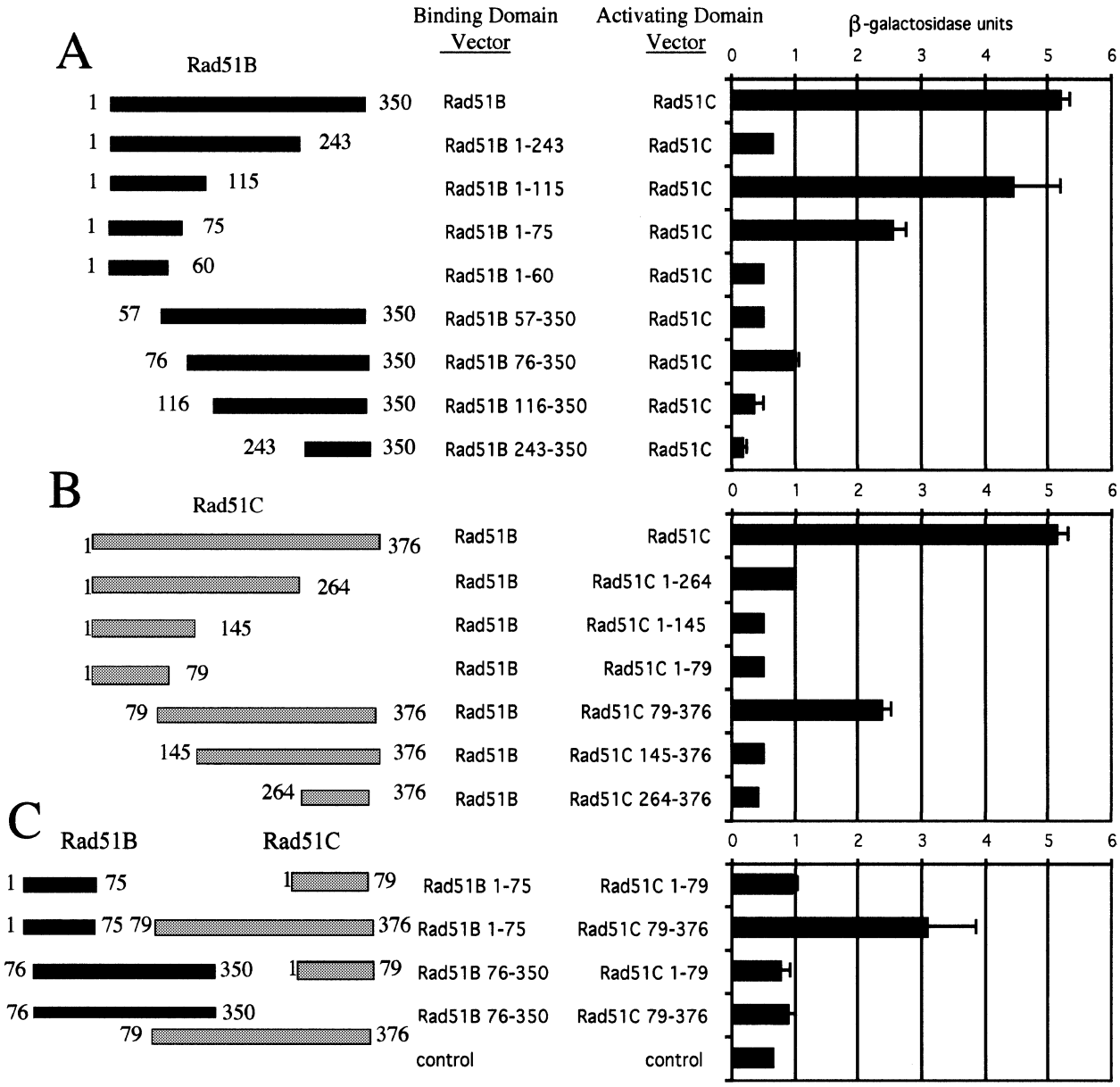

Figure 3. Deletion analysis of the Rad51B–Rad51C interaction. (**A**) Yeast two-hybrid assays were performed with full-length Rad51C in the activating domain vector and deletion constructs of Rad51B in the DNA binding domain vector from top to bottom: full-length Rad51B, $Rad51B_{1–243}$, $Rad51B_{1–115}$, $Rad51B_{1–75}$, $Rad51B_{1–60}$, $Rad51B_{57–350}$, $Rad51B_{76–350}$, $Rad51B_{116–350}$ and $Rad51B_{243–350}$. A schematic of the Rad51B fragments is on the left. On the right is the graph representing yeast two-hybrid results from liquid ONPG assays shown as β-galactosidase units. (**B**) Yeast were transformed with vectors containing full-length Rad51B in the DNA binding domain vector with deletion constructs of Rad51C in the activating domain vector from top to bottom: full-length Rad51C, $Rad51C_{1–264}$, $Rad51C_{1–145}$, $Rad51C_{1–79}$, $Rad51C_{79–376}$, $Rad51C_{145–376}$ and $Rad51C_{264–376}$. A schematic of the Rad51C fragments is on the left. A graph of results from liquid ONPG assays to determine β-galactosidase activity of each sample is on the right. (**C**) Yeast two-hybrid experiments were performed to test the Rad51B and Rad51C N- and C-terminal domains in all possible combinations. The N-terminal fragment of Rad51B with N- or C-terminal fragments of Rad51C and C-terminal fragment of Rad51B with N- or C-terminal fragments of Rad51C. Schematics of the fragments used are on the left. The pGBKT7 and pGADT7 are empty vectors for the binding domain and activating domain plasmids, respectively, and are shown as the control/control experiment. Results in all panels are from three experiments performed in triplicate with error bars showing standard deviation.

antibody. Thus, the co-immunoprecipitation experiments confirmed the yeast two-hybrid results.

In order to map the interactions of the other paralog proteins known to bind to Rad51C, yeast two-hybrid analysis was again employed. The full-length Xrcc3 was tested against the N- and C-terminal fragments of the Rad51C protein. Figure 5A demonstrates that Xrcc3 binds the C-terminal $Rad51C_{79–376}$, as does Rad51B, and Xrcc3 does not bind to the N-terminal fragment $Rad51C_{1–79}$. To confirm this interaction, baculovirus containing full-length Rad51C or $Rad51C_{79–376}$ was co-infected with Xrcc3 recombinant baculovirus into *Sf*21 insect cells. For these experiments, all proteins incorporate an N-terminal His tag and all recombinant proteins were expressed (Fig. 5B). Immunoprecipitation using an anti-Xrcc3 antibody showed that Xrcc3 binds to both the full-length Rad51C and $Rad51C_{79–376}$ proteins (Fig. 5C, lanes 1

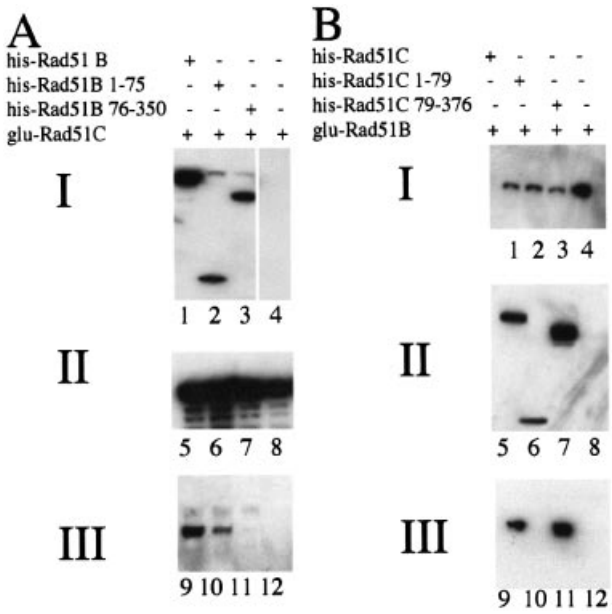

Figure 4. Biochemical analysis of the Rad51B–Rad51C interaction. (**A**) Insect cells were co-infected with baculovirus expressing Glu-tagged Rad51C alone (lane 4) or with full-length His–Rad51B (lane 1), His–Rad51B$_{1–75}$ (lane2) or His–Rad51B$_{76–350}$ (lane 3) as indicated with + or – symbols at the top of (I). (I) Western analysis with anti-His monoclonal antibody of co-infected insect cells detecting the His-tagged full-length Rad51B and Rad51B fragments. (II) Western analysis with anti-Rad51C monoclonal antibody detecting Glu–Rad51C. (III) Immunoprecipitation of His–Rad51B proteins with the anti-His antibody subsequently blotted with the anti-Rad51C monoclonal antibody. (**B**) Insect cells were co-infected with baculovirus expressing Glu-tagged Rad51B alone (lane 4) or with full-length His–Rad51C (lane 1), His–Rad51C$_{1–79}$ (lane 2) or His–Rad51C$_{70–376}$ (lane 3) as indicated with + or – symbols at the top of (I). (I) Western analysis using an anti-Rad51B polyclonal antibody detecting expression of Glu-tagged Rad51B in all four lanes. Rad51B is most highly expressed alone in lane 4. (II) Western analysis of the same lysates with anti-His monoclonal antibody to detect His–Rad51C (lane 1), His–Rad51C$_{1–79}$ (lane 2) or His–Rad51C$_{70–376}$ (lane 3). (III) Immunoprecipitation of samples with anti-His antibody followed by western blotting with anti-Rad51B polyclonal antibody.

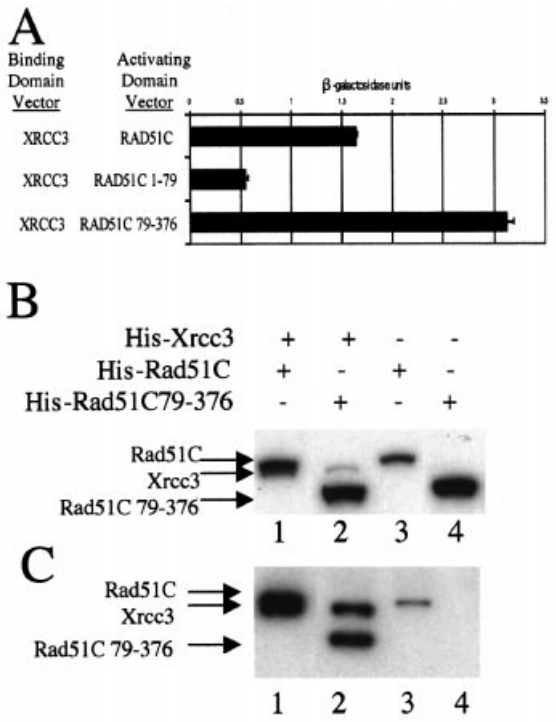

Figure 5. Mapping the Rad51C domain that interacts with Xrcc3. (**A**) Yeast two-hybrid analysis with vectors containing Xrcc3 in the DNA binding domain vector and full-length Rad51C, N-terminal fragment Rad51C$_{1–79}$ or C-terminal fragment Rad51C$_{79–376}$ in the activating domain vector was performed. β-Galactosidase activity was determined by liquid ONPG assay. Results shown are a representative experiment performed in triplicate. Error bars indicate standard deviation. (**B**) Biochemical analysis of the Rad51C–Xrcc3 interaction. Insect cells were co-infected with virus expressing His–Rad51C with His–Xrcc3 (lane 1), His–Rad51C$_{79–376}$ with His–Xrcc3 (lane 2), His–Rad51C (lane 3) or His–Rad51C$_{79–376}$ (lane 4) as indicated with + or – symbols at the top of this panel. Western blot with anti-His antibody detects expression of His-tagged proteins. Arrows indicate the position of each protein. His–Xrcc3 and His–Rad51C are very similar in molecular weight. (**C**) Immunoprecipitation with anti-Xrcc3 antibody of lysates shown in (B), followed by western blotting with anti-His antibody. Arrows indicate the position of each protein.

and 2). As both the Xrcc3 and Rad51C proteins were His tagged, they were both visualized on the blot (Fig. 5C, lanes 1 and 2). In addition, there was a small amount of Rad51C cross-reactivity with the Xrcc3 antibody in the immunoprecipitation (lane 3 in Fig. 5C), but the interaction between Rad51C$_{79–376}$ and Xrcc3 was clearly demonstrated as the specificity of the Rad51C fragment for Xrcc3 is shown in lane 2 and there is no cross-reactivity of this fragment with the Xrcc3 antibody (see lane 4).

Analysis of another Rad51C binding partner, Rad51D, yielded results similar to those with Rad51B and Xrcc3. The full-length mRad51D was tested against full-length Rad51C and the N- and C-terminal fragments of Rad51C by yeast two-hybrid analysis (Fig. 6A). The murine Rad51D sequence was used in these studies as it had optimal activity with Rad51C and Xrcc2 as compared with human Rad51D. Like Rad51B and Xrcc3, mRad51D bound to the C-terminal fragment of Rad51C$_{79–376}$ as well as full-length Rad51C while the N-terminal fragment Rad51C$_{1–79}$ did not bind to mRad51D. In addition, when the N- and C-terminal fragments of mRad51D were designed based on our homology model for Rad51D and tested for binding to full-length Rad51C. The large C-terminal fragment mRad51D$_{77–328}$ bound to Rad51C, and the N-terminal fragment mRad51D$_{4–77}$ did not bind to Rad51C (Fig. 6B). Finally, when the mRad51D fragments were tested against Xrcc2, the N-terminal fragment mRad51D$_{4–77}$ bound Xrcc2 while the C-terminal fragment mRad51D$_{77–328}$ did not bind to XRCC2 (Fig. 6C).

DISCUSSION

This study details the domain mapping of the BCDX2 and CX3 paralog protein complexes. Based on sequence homology to the *P.furiosus* Rad51 crystal structure, we have generated three-dimensional homology models for human Rad51B, Rad51C, Xrcc2, Xrcc3, and murine Rad51D. Based on these models, deletion mutants have been created to analyze the formation of the two major paralog protein complexes, BCDX2 and CX3.

Our models indicate the presence of an internal β-sheet within the C-terminus of the Rad51 paralog proteins, and the

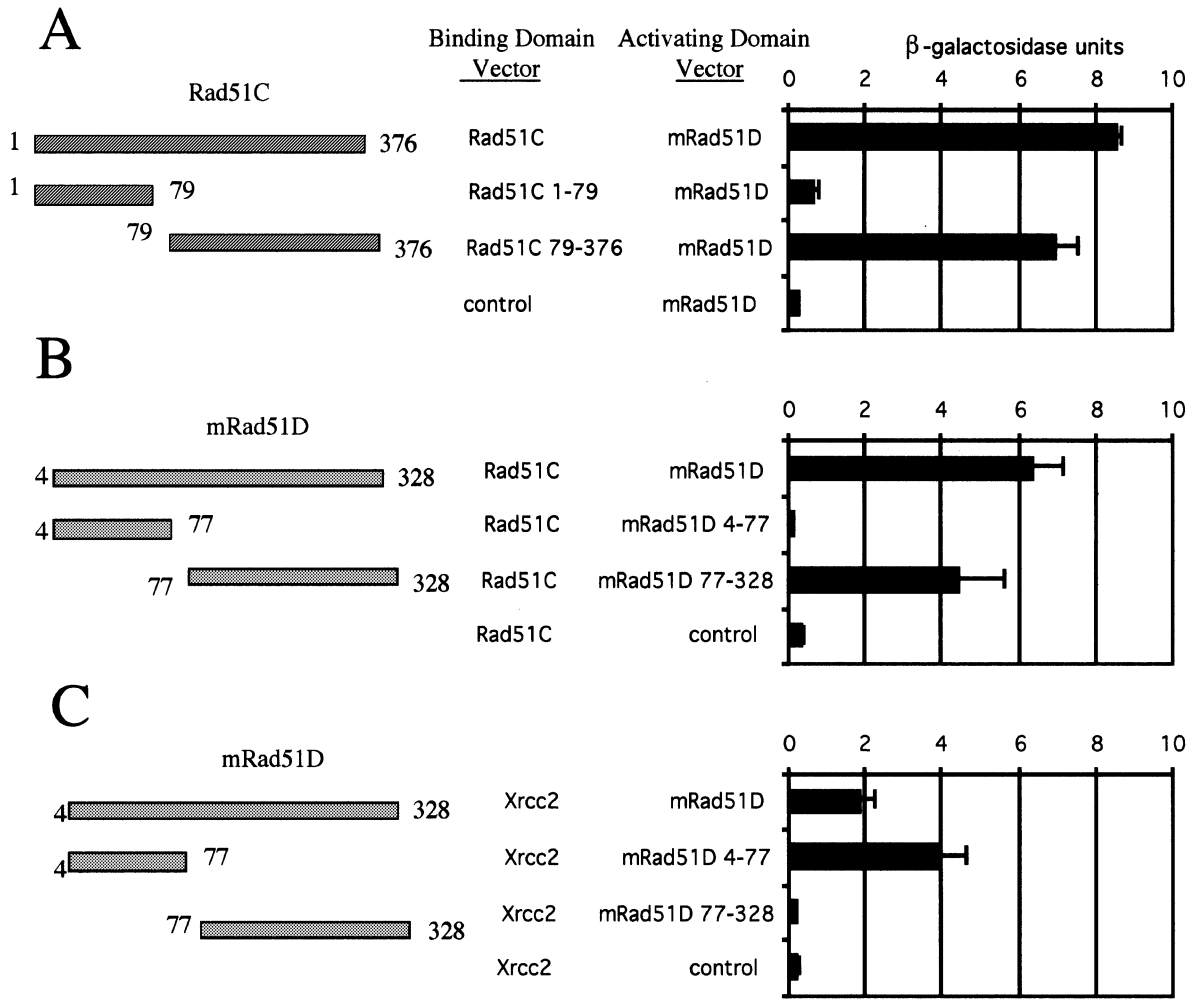

Figure 6. Domain mapping of mRad51D to Rad51C and Xrcc2. (**A**) Yeast two-hybrid analysis with vectors expressing full-length mRad51D in the GAL4 activating domain vector and full-length Rad51C or the Rad51C N- and C-terminal domains in the DNA binding vector. Empty DNA binding domain vector with mRad51D in the activating domain vector is shown as a negative control. A graph of results from liquid ONPG assays to determine β-galactosidase activity of each sample is on the right. Schematics for the Rad51C fragments are shown on the left. (**B**) Yeast two-hybrid analysis with full-length mRad51D, N-terminal domain $mRad51D_{4–77}$ or C-terminal domain $mRad51D_{77–328}$ co-transformed with Rad51C. Rad51C in the DNA binding vector with the empty activating domain vector is shown as a negative control. On the right is a graph of the results of β-galactosidase activity as determined by liquid ONPG assay. A schematic for the mRad51D fragments is shown on the left. (**C**) Yeast two-hybrid analysis of co-transformation of full-length mRad51D, N-terminal fragment $mRad51D_{4–77}$ or C-terminal fragment $mRad51D_{77–328}$ with Xrcc2. Xrcc2 alone is shown as a negative control. On the right is a graph of the results of the liquid ONPG assay used to determine β-galactosidase activity. The schematic of the mRad51D fragments is shown on the left. Results in all panels are from a representative experiment performed in triplicate with error bars showing standard deviation.

experiments here are consistent with the integrity of this sheet being critical to maintain that native protein fold. Since the order of the β-strands in space is not the same as their order in sequence, it is likely that fragments lacking any β-strand would fail to form the β-sheet resulting in a collapse of the protein core and misfolding of the protein. Consistently, Wong *et al.* found only a single fragment, out of five fragments tested, of the core domain of Rad51, i.e. $Rad51_{98–339}$, could bind to fragments of BRCA2 by yeast two-hybrid analysis (54); and, as it happens, this $Rad51_{98–339}$ fragment contains the entire internal β-sheet (54). There is additional evidence that the Rad51 paralogs (including Rad51) are particularly sensitive to deletions. A recent study of the binding of CX3 showed that only the first six amino acids could be removed from the N-terminus of Rad51C for detectable binding of RAD51C to Xrcc3 (37). A study by Dosanjh *et al.* also showed a truncated Rad51C protein containing amino acids 1–135 was also unable to bind Xrcc3 or Rad51B by yeast two-hybrid analysis (6).

Rad51C is central to both complexes and our results show that only the region of Rad51C containing residues 79–376 can bind to its protein partners, Rad51B, mRad51D and Xrcc3, through its C-terminal domain and linker region. Both the RecA filament (33) and the *Pf*Rad51 homo-heptamer (38) utilize a linker region for molecular interactions. Figure 7 illustrates a possible scheme for the binding of the paralog protein complexes, consistent with the experimental data presented here. In Figure 7, Xrcc2 is depicted as having no N-terminal domain, consistent with our sequence alignment (Fig. 1). We have shown that $Rad51B_{1–75}$ and not $Rad51B_{1–60}$ binds to Rad51C. These data suggest that this putative linker region connecting the N- and C-termini of Rad51B, residues

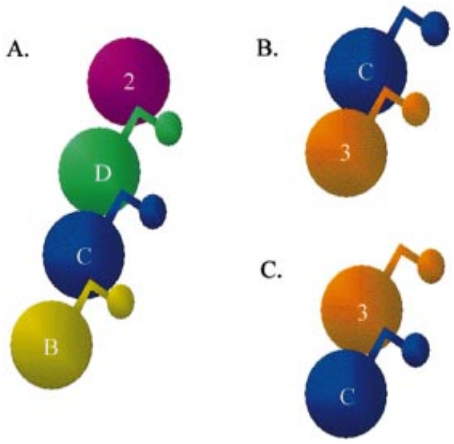

Figure 7. Schematic diagram of the binding architecture of the BCDX2 and CX3 complexes based on the models of the single proteins and the experimental data presented here. The large spheres are the C-terminal domains, while the small spheres represent the N-terminal domains (not present in Xrcc2). The linker regions are depicted as elbows between the spheres.

60–75, may be critical for the interaction of the Rad51B and Rad51C proteins. Our results also demonstrate that the murine $Rad51D_{4–77}$ fragment that also includes this linker region binds to full-length Xrcc2. A bold interpretation of our data would suggest that the BCDX2 complex is binding in the manner of the *Pf*Rad51 homo-heptamer or RecA filament where each paralog has developed a unique N-terminal linker that binds the C-terminal of its protein partner.

In the active deletion mutants of Rad51B and mRad51D, the linker region must be included with the N-terminus of both proteins. In the two binary complexes Rad51B–Rad51C and mRad51D–Xrcc2, only the N-termini and linker regions of Rad51B and mRad51D are required to bind to Rad51C and Xrcc2, respectively, as shown in Figure 7A. On the other hand, the fragment of Rad51C that binds to mRad51D contains the linker and C-terminal region suggesting the following two possibilities for the Rad51C–mRad51D complex in our model: either Rad51C uses its linker region to bind to mRad51D (as shown in Fig. 7A) in much the same way as the Rad51B–Rad51C and mRad51D–Xrcc2 complexes or the C-terminus of Rad51C binds to the C-terminus of mRad51D in a different manner from the *Pf*Rad51 homo-heptameric structure. The former hypothesis is supported by preliminary evidence that a point mutation (A87F, Miller,K.A. and Albala,J.S., unpublished results) in Rad51C abolishes binding of Rad51C to mRad51D but only partly disrupts the Rad51B–Rad51C complex. Kurumizaka *et al.* (37) showed that $Xrcc3_{63–346}$ and not $Xrcc3_{85–346}$ can bind to Rad51C. From these data, we infer that residues 63–85 of Xrcc3, like residues 60–75 of Rad51B, may be vital to the interaction with Rad51C. According to our model, residues 63–85 of Xrcc3 constitute the linker region, but it is likely that the linker region of Xrcc3 is not sufficient for binding to Rad51C, as it was demonstrated that Phe249 (which is in the C-terminal region of Xrcc3) is a critical amino acid for CX3 binding (37). It remains to be determined which linker region of Rad51C or Xrcc3, or both, is involved in CX3 complex formation (see Fig. 7B and C).

Our results suggest that the linker regions in the Rad51 paralog proteins may be critical for protein–protein interactions, and future characterization of these regions may help determine the exact points of contact between the proteins. Furthermore, *in vivo* examination of point mutations that alter complex formation will be useful in determining the importance of paralog complex formation in mediating Rad51 activity in DNA double-strand break repair.

SUPPLEMENTARY MATERIAL

Figure 1 is also available as a regular text file called Supplementary Material Figure S2 at NAR Online.

ACKNOWLEDGEMENTS

We wish to thank David Shin and John A. Tainer for sharing their coordinates of their *P.furiosus* Rad51 crystal structure with us prior to publication. The authors acknowledge Marianne Kavanagh, Lynae Brown, Ceslovas Venclovas and Adam Zemla for technical assistance. The authors would like to thank Daniel Yoshikawa and Ian McConnell for critical review of the manuscript. The authors would like to thank David Schild for the yeast two-hybrid vectors, Larry Thompson for the Xrcc3 cDNA and Doug Pittman for the murine Rad51D cDNA plasmid. This work was funded by NIH grant CA-81019-02 awarded to J.S.A. This work was performed under the auspices of the U.S. Department of Energy by the UC-LLNL under Contract No. W-7405-Eng-48.

REFERENCES

1. Shinohara,A. and Ogawa,T. (1995) Homologous recombination and the roles of double-strand breaks. *Trends Biochem. Sci.*, **20**, 387–391.
2. Sung,P. (1994) Catalysis of ATP-dependent homologous DNA pairing and strand exchange by yeast RAD51 protein. *Science*, **265**, 1241–1243.
3. Sung,P. (1997) Yeast Rad55 and Rad57 proteins form a heterodimer that functions with replication protein A to promote DNA strand exchange by Rad51 recombinase. *Genes Dev.*, **11**, 1111–1121.
4. Ogawa,T., Yu,X., Shinohara,A. and Egelman,E.H. (1993) Similarity of the yeast RAD51 filament to the bacterial RecA filament. *Science*, **259**, 1896–1899.
5. Pittman,D.L., Weinberg,L.R. and Schimenti,J.C. (1998) Identification, characterization and genetic mapping of Rad51d, a new mouse and human RAD51/RecA-related gene. *Genomics*, **49**, 103–111.
6. Dosanjh,M.K., Collins,D.W., Fan,W., Lennon,G.G., Albala,J.S., Shen,Z. and Schild,D. (1998) Isolation and characterization of RAD51C, a new human member of the RAD51 family of related genes. *Nucleic Acids Res.*, **26**, 1179–1184.
7. Cartwright,R., Tambini,C.E., Simpson,P.J. and Thacker,J. (1998) The XRCC2 DNA repair gene from human and mouse encodes a novel member of the recA/RAD51 family. *Nucleic Acids Res.*, **26**, 3084–3089.
8. Albala,J.S., Thelen,M.P., Prange,C., Fan,W., Christensen,M., Thompson,L.H. and Lennon,G.G. (1997) Identification of a novel human RAD51 homolog, RAD51B. *Genomics*, **46**, 476–479.
9. Rice,M.C., Smith,S.T., Bullrich,F., Havre,P. and Kmiec,E.B. (1997) Isolation of human and mouse genes based on homology to REC2, a recombinational repair gene from the fungus *Ustilago maydis*. *Proc. Natl Acad. Sci. USA*, **94**, 7417–7422.
10. Liu,N., Lamerdin,J.E., Tebbs,R.S., Schild,D., Tucker,J.D., Shen,M.R., Brookman,K.W., Siciliano,M.J., Walter,C.A., Fan,W. *et al.* (1998) XRCC2 and XRCC3, new human Rad51-family members, promote chromosome stability and protect against DNA cross-links and other damages. *Mol. Cell*, **1**, 783–793.
11. Tambini,C.E., George,A.M., Rommens,J.M., Tsui,L.C., Scherer,S.W. and Thacker,J. (1997) The XRCC2 DNA repair gene: identification of a positional candidate. *Genomics*, **41**, 84–92.

12. Tebbs,R.S., Zhao,Y., Tucker,J.D., Scheerer,J.B., Siciliano,M.J., Hwang,M., Liu,N., Legerski,R.J. and Thompson,L.H. (1995) Correction of chromosomal instability and sensitivity to diverse mutagens by a cloned cDNA of the XRCC3 DNA repair gene. *Proc. Natl Acad. Sci. USA*, **92**, 6354–6358.
13. Cartwright,R., Dunn,A.M., Simpson,P.J., Tambini,C.E. and Thacker,J. (1998) Isolation of novel human and mouse genes of the recA/RAD51 recombination-repair gene family. *Nucleic Acids Res.*, **26**, 1653–1659.
14. Pittman,D.L. and Schimenti,J.C. (2000) Midgestation lethality in mice deficient for the RecA-related gene, Rad51d/Rad51l3. *Genesis*, **26**, 167–173.
15. Shu,Z., Smith,S., Wang,L., Rice,M.C. and Kmiec,E.B. (1999) Disruption of muREC2/RAD51L1 in mice results in early embryonic lethality which can be partially rescued in a p53(–/–) background. *Mol. Cell. Biol.*, **19**, 8686–8693.
16. Deans,B., Griffin,C.S., Maconochie,M. and Thacker,J. (2000) Xrcc2 is required for genetic stability, embryonic neurogenesis and viability in mice. *EMBO J.*, **19**, 6675–6685.
17. Takata,M., Sasaki,M.S., Sonoda,E., Fukushima,T., Morrison,C., Albala,J.S., Swagemakers,S.M., Kanaar,R., Thompson,L.H. and Takeda,S. (2000) The Rad51 paralog Rad51B promotes homologous recombinational repair. *Mol. Cell. Biol.*, **20**, 6476–6482.
18. Takata,M., Sasaki,M.S., Tachiiri,S., Fukushima,T., Sonoda,E., Schild,D., Thompson,L.H. and Takeda,S. (2001) Chromosome instability and defective recombinational repair in knockout mutants of the five Rad51 paralogs. *Mol. Cell. Biol.*, **21**, 2858–2866.
19. Griffin,C.S., Simpson,P.J., Wilson,C.R. and Thacker,J. (2000) Mammalian recombination-repair genes XRCC2 and XRCC3 promote correct chromosome segregation. *Nature Cell Biol.*, **2**, 757–761.
20. Schild,D., Lio,Y., Collins,D.W., Tsomondo,T. and Chen,D.J. (2000) Evidence for simultaneous protein interactions between human Rad51 paralogs. *J. Biol. Chem.*, **275**, 16443–16449.
21. Sigurdsson,S., Van Komen,S., Bussen,W., Schild,D., Albala,J.S. and Sung,P. (2001) Mediator function of the human Rad51B-Rad51C complex in Rad51/RPA-catalyzed DNA strand exchange. *Genes Dev.*, **15**, 3308–3318.
22. Miller,K.A., Yoshikawa,D.M., McConnell,I.R., Clark,R., Schild,D. and Albala,J.S. (2002) RAD51C interacts with RAD51B and is central to a larger protein complex *in vivo* exclusive of RAD51. *J. Biol. Chem.*, **277**, 8406–8411.
23. Kurumizaka,H., Ikawa,S., Nakada,M., Enomoto,R., Kagawa,W., Kinebuchi,T., Yamazoe,M., Yokoyama,S. and Shibata,T. (2002) Homologous pairing and ring and filament structure formation activities of the human Xrcc2*Rad51D complex. *J. Biol. Chem.*, **277**, 14315–14320.
24. Braybrooke,J.P., Spink,K.G., Thacker,J. and Hickson,I.D. (2000) The RAD51 family member, RAD51L3, is a DNA-stimulated ATPase that forms a complex with XRCC2. *J. Biol. Chem.*, **275**, 29100–29106.
25. Masson,J.Y., Tarsounas,M.C., Stasiak,A.Z., Stasiak,A., Shah,R., McIlwraith,M.J., Benson,F.E. and West,S.C. (2001) Identification and purification of two distinct complexes containing the five RAD51 paralogs. *Genes Dev.*, **15**, 3296–3307.
26. Wiese,C., Collins,D.W., Albala,J.S., Thompson,L.H., Kronenberg,A. and Schild,D. (2002) Interactions involving the Rad51 paralogs Rad51C and XRCC3 in human cells. *Nucleic Acids Res.*, **30**, 1001–1008.
27. Liu,N., Schild,D., Thelen,M.P. and Thompson,L.H. (2002) Involvement of Rad51C in two distinct protein complexes of Rad51 paralogs in human cells. *Nucleic Acids Res.*, **30**, 1009–1015.
28. Lio,Y.C., Mazin,A.V., Kowalczykowski,S.C. and Chen,D.J. (2003) Complex formation by the human Rad51B and Rad51C DNA repair proteins and their activities *in vitro*. *J. Biol. Chem.*, **278**, 2469–2478.
29. Masson,J.Y., Stasiak,A.Z., Stasiak,A., Benson,F.E. and West,S.C. (2001) Complex formation by the human RAD51C and XRCC3 recombination repair proteins. *Proc. Natl Acad. Sci. USA*, **98**, 8440–8446.
30. Yokoyama,H., Kurumizaka,H., Ikawa,S., Yokoyama,S. and Shibata,T. (2003) Holliday junction binding activity of the human Rad51B protein. *J. Biol. Chem.*, **278**, 2767–2772.
31. Coleman,M.A., Miller,K.A., Beernink,P.T., Yoshikawa,D.M. and Albala,J.S. (2003) Identification of chromatin-related protein interactions using protein microarrays. *Proteomics*, **3**, 2101–2107.
32. Story,R.M. and Steitz,T.A. (1992) Structure of the recA protein–ADP complex. *Nature*, **355**, 374–376.
33. Story,R.M., Weber,I.T. and Steitz,T.A. (1992) The structure of the *E. coli* recA protein monomer and polymer. *Nature*, **355**, 318–325.
34. Aihara,H., Ito,Y., Kurumizaka,H., Yokoyama,S. and Shibata,T. (1999) The N-terminal domain of the human Rad51 protein binds DNA: structure and a DNA binding surface as revealed by NMR. *J. Mol. Biol.*, **290**, 495–504.
35. Pellegrini,L., Yu,D.S., Lo,T., Anand,S., Lee,M., Blundell,T.L. and Venkitaraman,A.R. (2002) Insights into DNA recombination from the structure of a RAD51–BRCA2 complex. *Nature*, **420**, 287–293.
36. Krejci,L., Damborsky,J., Thomsen,B., Duno,M. and Bendixen,C. (2001) Molecular dissection of interactions between Rad51 and members of the recombination-repair group. *Mol. Cell. Biol.*, **21**, 966–976.
37. Kurumizaka,H., Enomoto,R., Nakada,M., Eda,K., Yokoyama,S. and Shibata,T. (2003) Region and amino acid residues required for Rad51C binding in the human Xrcc3 protein. *Nucleic Acids Res.*, **31**, 4041–4050.
38. Shin,D.S., Pellegrini,L., Daniels,D.S., Yelent,B., Craig,L., Bates,D., Yu,D.S., Shivji,M.K., Hitomi,C., Arvai,A.S., Volkmann,N., Tsuruta,H., Blundell,T.L., Venkitaraman,A.R. and Tainer,J.A. (2003) Full-length archaeal Rad51 structure and mutants: mechanisms for RAD51 assembly and control by BRCA2. *EMBO J.*, **22**, 4566–4576.
39. Venclovas,C. (2001) Comparative modeling of CASP4 target proteins: combining results of sequence search with three-dimensional structure assessment. *Proteins: Struct. Func. Genet.*, **Suppl. 5**, 47–54.
40. Sauder,J.M., Arthur,J.W. and Dunbrack,R.L. (2000) Large-scale comparison of protein sequence alignment algorithms with structure alignments. *Proteins: Struct. Func. Genet.*, **40**, 6–22.
41. Chothia,C. and Lesk,A.M. (1986) The relation between the divergence of sequence and structure in proteins. *EMBO J.*, **5**, 823–826.
42. Lennon,G., Auffray,C., Polymeropoulos,M. and Soares,M.B. (1996) The I.M.A.G.E. Consortium: an integrated molecular analysis of genomes and their expression. *Genomics*, **33**, 151–152.
43. Altschul,S.F., Madden,T.L., Schäffer,A.A., Zhang,J., Zhang,Z., Miller,W. and Lipman,D.J. (1997) Gapped BLAST and PSI-BLAST: a new generation of protein database search programs. *Nucleic Acids Res.*, **25**, 3389–3402.
44. Walker,D.R. and Koonin,E.V. (1997) SEALS: a system for easy analysis of lots of sequences. *Proc. Int. Conf. Intell. Syst. Mol. Biol.*, **5**, 333–339.
45. Sali,A. and Blundell,T.L. (1993) Comparative protein modelling by satisfaction of spatial restraints. *J. Mol. Biol.*, **234**, 779–815.
46. McGuffin,L.J., Bryson,K. and Jones,D.T. (2000) The PSIPRED protein structure prediction server. *Bioinformatics*, **16**, 404–405.
47. Berman,H.M., Westbrook,J., Feng,Z., Gilliland,G., Bhat,T.N., Weissig,H., Shindyalov,I.N. and Bourne,P.E. (2000) The Protein Data Bank. *Nucleic Acids Res.*, **28**, 235–242.
48. Sawaya,M.R., Guo,S., Tabor,S., Richardson,C.C. and Ellenberger,T. (1999) Crystal structure of the helicase domain from the replicative helicase-primase of bacteriophage T7. *Cell*, **99**, 167.
49. Holm,L. and Sander,C. (1996) Mapping the protein universe. *Science*, **273**, 595–603.
50. Dunbrack,R.L.J. and Karplus,M. (1993) Backbone-dependent rotamer library for proteins. Application to side-chain prediction. *J. Mol. Biol.*, **230**, 543–571.
51. Sippl,M.J. (1993) Recognition of errors in 3-dimensional structures of proteins. *Proteins*, **17**, 355–362.
52. Kabsch,W. and Sander,C. (1983) Dictionary of protein secondary structure—pattern-recognition of hydrogen-bonded and geometrical features. *Biopolymers*, **22**, 2577–2637.
53. Brendel,V., Brocchieri,L., Sandler,S.J., Clark,A.J. and Karlin,S. (1997) Evolutionary comparisons of Reca-like proteins across all major kingdoms of living organisms. *J. Mol. Evol.*, **44**, 528–541.
54. Wong,A.K.C., Pero,R., Ormonde,P.A., Tavtigian,S.V. and Bartel,P.L. (1997) RAD51 interacts with the evolutionarily conserved BRC motifs in the human breast cancer susceptibility gene brca2. *J. Biol. Chem.*, **272**, 31941–31944.
55. Kraulis,P.J. (1991) Molscript—a program to produce both detailed and schematic plots of protein structures. *J. Appl. Crystallogr.*, **24**, 946–950.
56. Merritt,E.A. and Bacon,D.J. (1997) *Macromolecular Crystallography*, *Part B*. Academic Press, San Diego, CA, Vol. 277, pp. 505–524.
57. Somoza,J.R., Menon,S., Schmidt,H., Joseph-McCarthy,D., Dessen,A., Stahl,M.L., Somers,W.S. and Sullivan,F.X. (2000) Structural and kinetic analysis of *Escherichia coli* GDP-mannose 4,6-dehydratase provides insights into the enzyme's catalytic mechanism and regulation by GDP-fucose. *Struct. Fold. Design*, **8**, 123–135.